physica status solidi a
www.pss-a.com
applications and materials science

Metal/Organic Interface Formation Studied *in situ* by Resonant Raman Spectroscopy

G. Salvan[1], B.A. Paez[1], D.R.T. Zahn[1], L. Gisslen[2], R. Scholz[2]

[1] Institut für Physik, Technische Universität Chemnitz, D-09107 Chemnitz, Germany
[2] Walter Schottky Institut, Technische Universität München, Am Coulombwall 3, D-85748 Garching, Germany

Received zzz, revised zzz, accepted zzz
Published online zzz

PACS 00.00.Xx, 11.11.Yy

Novel devices based on organic semiconductors such as organic field effect transistors require metallic contacts. Therefore the interface between metals and organic semiconductors deserves special attention. Here *in situ* Raman scattering was applied to assess metal/organic interface formation. As model systems the deposition of Ag, In, and Mg onto molecular layers of two perylene derivatives, PTCDA and DiMe-PTCDI was investigated. The results provide information on the chemical aspects of the interface formation as well as on the indifussion of the metal atoms into the organic layers.

1 Introduction In recent years, enormous progress was made in the understanding of organic semiconductors. The research interest in these materials is driven by the various applications ranging from organic light emitting devices (OLEDs) over organic field effect transistors (OFETs) to organic photovoltaic cells (OPVCs). Experimental techniques such as photoemission spectroscopy which has been one major surface science technique in the field of inorganic semiconductor research for decades has also been successfully applied to study organic semiconductors and their interfaces for quite some time. Other experimental techniques such as Raman spectroscopy are less widely used for studying organic semiconductor interfaces. However, also this optical spectroscopy technique, which probes the vibrational modes and may thus also be called vibrational spectroscopy, can provide very valuable information about interface properties such as geometric structure, band bending, and interfacial chemistry. It is the intention of this review to illustrate that Raman spectroscopy can contribute significantly to the field of organic interface characterisation by providing an insight in the chemistry and structural aspects of the organic interface formation.

2 Methods

2.1 Sample preparation and characterization

The organic layers were grown onto sulfur-passivated GaAs(100) substrates by organic molecular beam deposition (OMBD) in an ultra high vacuum chamber (UHV) with $7 \cdot 10^{-10}$ mbar base pressure. The passivation procedure is described in reference [1].

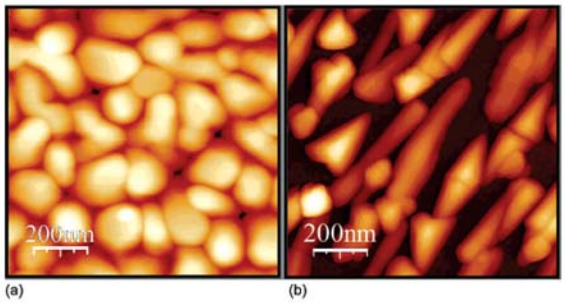

Fig. 1 AFM images of PTCDA (a) and DiMePTCDI (b) films with a nominal thickness of 20 nm grown on S-GaAs(100).

The molecular materials obtained from Syntec GmbH

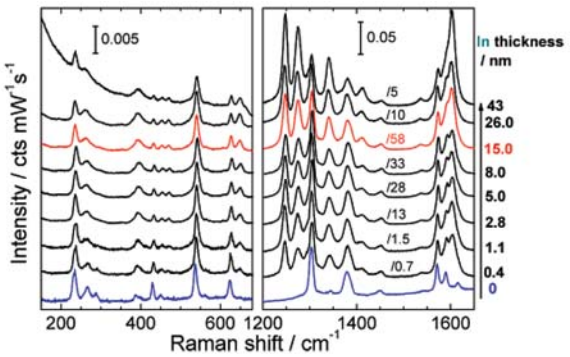

Fig. 2 Raman spectra of PTCDA acquired upon successive deposition of In onto a 15 nm PTCDA film. The spectra normalization is done with respect to the intensity of the C-C stretch modes (1572 cm^{-1}).

Wolfen were pre-purified by a two step sublimation prior to the deposition. The organic materials and the metals were evaporated from Knudsen cells kept at 280°C for PTCDA, 270°C for DiMe-PTCDI, 930°C for Ag, 830°C for In, and at 375°C for Mg, resulting in deposition rates of 0.3 nm/min for both perylene derivatives, 1.6 nm/min for Ag and 2 nm/min for In and Mg. During the growth of these films, the substrates were kept at room temperature.

The films consist of islands (see AFM images in Fig. 1) the crystalline character of which was proven by Raman spectroscopy [2].

For the *in situ* Raman measurements, the UHV system is optically aligned with a triple monochromator Raman spectrometer (Dilor XY) equipped with a CCD camera for multichannel detection [1]. The samples were excited with the 488 nm (2.54 eV) Ar^+ laser line that lies in the first absorption maximum of both organic molecules and thus ensures resonance conditions for the Raman process.

2.2 Theoretical methods

The ground state geometries of the molecules are optimized with density functional theory (DFT), and the geometries in the excited states with time-dependent density functional theory (TD-DFT). As discussed elsewhere, the deformation patterns can be understood from the changes of the node patterns of the two electronic orbitals involved in the dipole-active transition, in our cases the highest occupied molecular orbital (HOMO) and the lowest unoccupied orbital (LUMO) [3,4]. For each compound, the deformation pattern between the geometries in the relaxed excited state and in the ground state is projected onto the vibrational eigenvectors obtained on the potential energy surface of the ground state. All calculations are performed with the program packages Gaussian98 [5] and turbomole5.7 [6], using the hybrid functional B3LYP and localized basis sets.

3 Results and discussions

3.1 Chemistry of metal/organic interfaces

Two spectral regions were recorded upon step-wise metal deposition. The region between 25 cm^{-1} and 650 cm^{-1} contains a mode corresponding to the breathing of the whole molecule and C-C stretching modes [7]. The frequency region between 1200 cm^{-1} and 1650 cm^{-1} contains internal modes with C-H and C-C character. Fig. 1 shows the Raman spectrum of a bare 15 nm PTCDA film and its evolution upon the step-wise deposition of indium.

The overall signal intensity increases with the In thickness up to 15 nm and decreases for higher metal coverages as shown by the normalization factors in Fig. 2. The same behaviour is observed when Ag is deposited onto PTCDA and for both metals deposited onto DiMe-PTCDI [8, 9].

This effect is known as surface enhanced Raman scattering (SERS) [10, 11, 12]. The SERS effect has been widely investigated for various molecules adsorbed on rough metallic surfaces or on metallic clusters in colloids. Reviews on this topic can be found in references [12, 13, 14, 15]. The enhancement of normally Raman-active modes is a consequence of the enhancement of the electric field of the incoming and scattered radiation in the vicinity of a rough metal film upon coupling with the dipolar plasmon resonances in the metal clusters. This enhancement affects molecules located up to even 10 nm away from the metal surface [11, 12]. The enhancement factors are essentially determined by the electronic properties of the metal and by the morphology of the metal film.

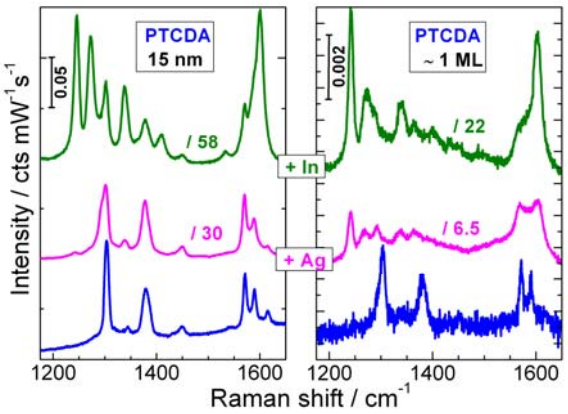

Fig. 3 Raman spectra of a 15 nm (left) and of a ML (right) PTCDA film clean (bottom) and covered with nominally 15 nm of silver (middle) and indium (top) each.

In addition to the enhancement of the totally symmetric Raman active modes, already the deposition of only 0.4 nm In leads to the appearance of some modes in the higher frequency region. The same modes were also observed when depositing In or Ag onto a ML of PTCDA on S-GaAs, only with different relative intensities (Fig. 3). They therefore are a signature of the molecules in direct contact or in the very near vicinity of a metal surface. In general,

such a break-down of the selection rules accompanies the SERS effect and can be induced by several mechanisms: structural deformation of the molecule, charge transfer from the molecule into the metal or *vice versa*, or formation of new chemical bonds. Thus the spectral changes induced by SERS can be used to extract information about chemical reactions at the interface, as well as about the morphology of the metal film.

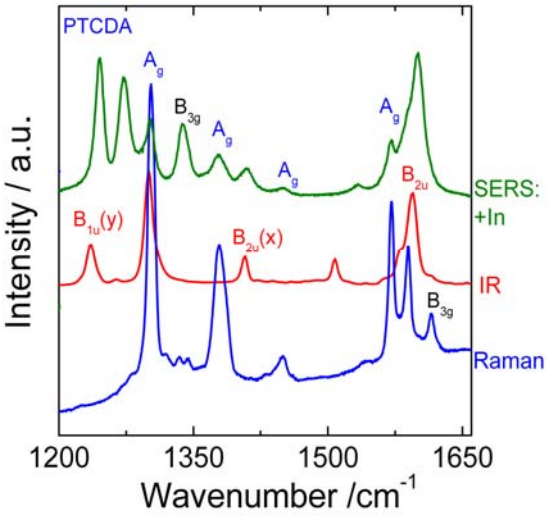

Fig. 4 Example of the activation of infrared active modes in the Raman spectrum for the case of indium deposition onto PTCDA..

The band at 1338 cm^{-1} was identified in reference [16] to be a B_{3g} band based on its frequency and intensity in the crystal spectra, while a band 1292 cm^{-1} is likely to be a shifted variant of the C-H deformation A_g mode at 1303 cm^{-1} in the single crystal [17]. The other bands correspond to modes which normally show infrared activity (see Fig. 4). Considering that all the modes occurring upon In and Ag deposition are normal modes of the PTCDA molecule, the observed break-down of the Raman-infrared selection rules was proposed to originate from a weak charge transfer between the molecules and the metal surface mediated by molecular vibrations [9].

This is in contradiction to previous findings of Hirose *et al*. [18] and Kera *et al*. [19] who proposed the formation of a In_4PTCDA complex.

In order to assess the effect of a metal-PTCDA complex formation on the vibrational frequencies theoretical calculations were preformed with the Gaussian'98 package on the In_4PTCDA complex using the B3LYP functional and the basis set LANL2DZ which takes into account possible relativistic effects due to the presence of the heavy metal atoms [5]. Four In atoms were assumed to interact with the PTCDA molecule via the O atoms in the anhydride groups according to reference [19]. The optimised geometry, the electronic levels and the charge distribution over the complexes are similar to those reported in reference [19]. Fig. 5 shows the spectrum of a PTCDA single crystal together with the calculated frequencies for a single PTCDA molecule (rhombus) and for an In_4PTCDA complex (triangles).

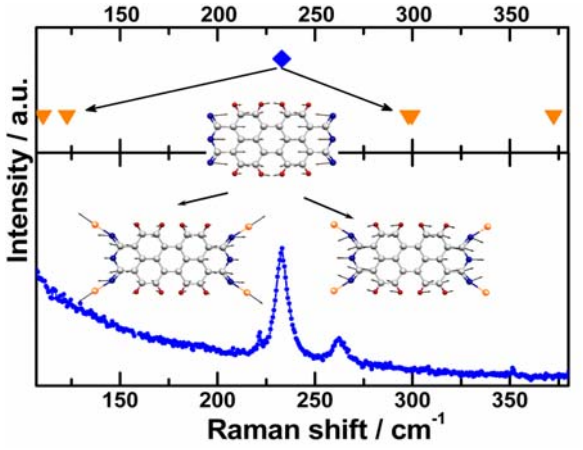

Fig. 5 Raman spectrum of a PTCDA crystal along with calculated frequencies for a single molecule (rhombus) and for a In_4PTCDA complex (triangles).

The most dramatic effect of the complex formation resides in the two-fold splitting of the breathing mode at 233 cm^{-1} (see the elongation patterns in Fig. 5). A first component originates from a breathing of the whole complex and the significant increment of mass compared to the single PTCDA molecule results in a dramatic shift towards lower frequencies (110 cm^{-1}). For the second component the In atoms are fixed and constrain the breathing of the PTCDA molecule increasing its frequency to 299 cm^{-1}. In the experimental Raman spectra (Fig. 1) of the In/PTCDA heterostructure, the molecular breathing mode is still observed at 233 cm^{-1}, ruling out the possibility of this chemical reaction. This conclusion is further supported by infrared spectroscopy studies [9] and by recent high resolution PES results [2].

In Fig. 6 the Raman spectra of 15 nm films of PTCDA are shown for metal coverages of 5 nm In, 4.5 nm Ag, and 5 nm Mg. The spectra in the low frequency windows are normalized to the height of the molecular breathing mode at 233 cm^{-1}. The normalization in the high frequency region is again performed with respect to the C=C stretching mode (1572 cm^{-1}).

The Raman spectra of the (5 nm) Mg/(15 nm) PTCDA system also exhibit the break-down of selection rules, with the occurrence of the modes observed in the other two metal/organic heterostructures (see Fig. 6). In addition, several modes with significant intensity (marked with asterisks in Fig. 6) appear at: 307 cm^{-1}, 502 cm^{-1}, 598 cm^{-1}, 696 cm^{-1}, 1088 cm^{-1} as well as at 1225 cm^{-1} and 1433 cm^{-1}. The frequency of the mode at 598 cm^{-1} is very close to the calculated value of 592 cm^{-1} for a B_{3g} mode of an isolated PTCDA molecule [4].

Frequency calculations performed with the same basis set and density functional methods in Gaussian'98 as in ref. [4] but for a modified PTCDA molecule, in which the central O atom in the anhydride group is removed, deliver several frequencies that may be candidates for the assignment of the experimentally observed modes: 308 cm^{-1}, 500 cm^{-1}, 581 cm^{-1}, 702 cm^{-1}, 1090 cm^{-1}. Raman active modes in MgO microcrystals [20] were observed at 595 cm^{-1}, 719 cm^{-1} and 1096 cm^{-1}. Thus the modes observed in the present work at 598 cm^{-1}, 696 cm^{-1} and 1088 cm^{-1} are very likely to indicate the formation of MgO as a result of the interaction between Mg and PTCDA. No modes of PTCDA or the modified molecule are found in the vicinity of 1225 cm^{-1}.

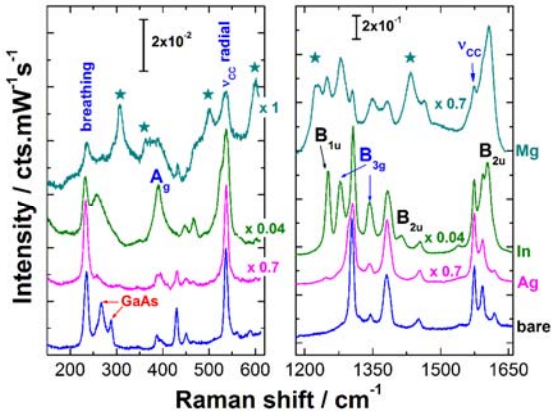

Fig. 6 Raman spectra for In (5nm), Ag (4,5 nm) and Mg (5 nm) coverages on 15 nm thick PTCDA films, compared with the spectrum of the bare PTCDA film in the spectral region of the internal breathing mode (left) and in the spectral region of C-H deformation and C=C stretching modes (right)..

Whatever the final assignment of the new modes is, they are not activated in the molecules in contact with either Ag or with In. Therefore it can be concluded that the model of weak charge transfer is not sufficient to describe the interaction at the Mg/PTCDA interface.

To validate the model deduced from the results of these Raman spectroscopy experiments detailed investigations of the Mg/PTCDA system by means of other methods that are highly sensitive with respect to the changes of the chemical environment and charge redistribution such as photoemission spectroscopy were performed [2].

In Fig. 7 the spectra of 15 nm DiMe-PTCDI films for metal coverages of 5nm In, 4.5 nm Ag and 5 nm Mg are shown. The spectra in the low frequency windows are normalized to the height of the breathing mode at 221 cm^{-1}. The normalization in the high frequency region is performed with respect to the C-C stretching mode (1570 cm^{-1}).

In the case of DiMe-PTCDI all the investigated metals, *i.e.* Ag, In and Mg, lead to the break-down of selection rules with the occurrence of normally infrared active modes at 1246 cm^{-1} and 1606 cm^{-1}. The breathing mode at 221 cm^{-1} survives with increasing metal coverage. Thus a chemical reaction between these metals and the O atoms of DiMe-PTCDI molecules can again be ruled out. Interestingly, the features potentially assigned to MgO phonons do not appear in the spectra even for higher coverages of Mg. It can thus be concluded that the methylimide group in the DiMe-PTCDI molecule is less reactive compared to the O atoms in the anhydride group of PTCDA.

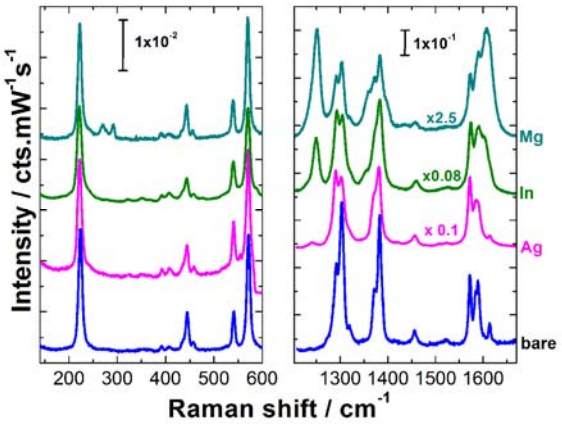

Fig. 7 Raman spectra for In (5nm), Ag (4,5 nm) and Mg (6 nm) coverages on 15 nm thick DiMe-PTCDI films, compared with the spectrum of the bare DiMe-PTCDI film.

3.2 Morphological Properties and Indiffusion of Metals at the Interfaces with Organic Semiconductors

Besides the occurrence of internal modes related to molecules in direct contact with the metal the totally symmetric modes are also enhanced (as shown by the normalization factors in Fig. 8 (a) and (b)) in the spectra of Ag, In and Mg on 15 nm thick PTCDA and DiMe-PTCDI films.

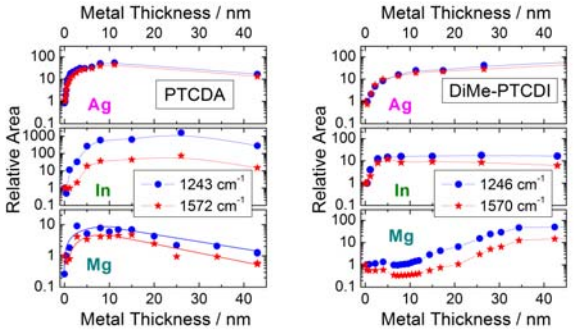

Fig. 8 Enhancement factors of the B_u mode (1243 cm^{-1} in PTCDA and 1246 cm^{-1} in DiMe-PTCDI) and of the C-C stretching A_g mode (1572 cm^{-1} in PTCDA and 1570 cm^{-1} in DiMe-PTCDI) for PTCDA (a) and DiMe-PTCDI (b) as a function of the metal coverage.

The latter effect originates from the coupling between the incident and scattered radiation with localized and/or collective plasmon resonances in the rough metal film. Therefore the intensity of the totally symmetric A_g modes is very sensitive to the morphology of the metal film.

For a quantitative determination of the enhancement factors curve fitting of each set of spectra recorded during silver, indium and magnesium deposition onto PTCDA and DiMe-PTCDI was performed using Lorentzian peaks. The dependence of relative area on metal coverage is plotted in Fig. 6 for a representative totally symmetric mode and for a normally infrared active mode of each organic material. The relative intensities were calculated by dividing the intensities in the spectra at a given coverage to the initial intensities in the spectrum where the mode occurs for the first time. For example, the reference spectrum for the totally symmetric Raman band is that of the pure organic film, while the reference spectrum for normally infrared active band is that taken after the first metal deposition.

The intensities of the A_g modes initially increase upon Ag and In deposition reflecting an increase in number and size of metal clusters as their plasmon energy approaches the energy of the laser electromagnetic field. When Mg is deposited onto PTCDA the intensities initially decrease, reflecting a reduction in number of Raman active PTCDA molecules. This is in good agreement with the conclusion drawn in the previous section regarding the disruption of PTCDA molecular structure upon reaction with Mg. In the next deposition step, *i.e.* at 2.8 nm Mg nominal coverage, the A_g Raman modes start to be enhanced indicating the formation of metallic clusters. The enhancement of the totally symmetric modes of DiMe-PTCDI occurs only above 15 nm nominal Mg thickness.

The PES studies (see ref. [2]) showed that the metallic character of Mg clusters occurs at coverages above 1.6 nm for PTCDA and between 9 and 15 nm for DiMe-PTCDI. The large difference in the nominal thickness for which the metallic character of Mg clusters is formed on the two molecules is probably related to the different morphology of the underlying organic layer. The DiMe-PTCDI films have very large voids between the organic islands, while the PTCDA films are much more compact (see Fig. 1).

The maximum enhancement of PTCDA modes for the Ag/PTCDA (15 nm) system is observed around 11 nm nominal Ag coverage (Fig. 8 (a)) and corresponds to the optimum cluster size for the dipolar plasmon resonance. The In film thicknesses yielding the maximum enhancement for PTCDA and DiMe-PTCDI films are 26 nm and 5 nm, respectively. Further increase in the metal thickness leads to increasing size of the metal clusters associated with decreasing strength of the plasmon coupling with the incident and scattered radiation. Furthermore, the absorption in the metal film also plays an important role in decreasing the Raman signal for higher nominal coverages, when the clusters start to percolate.

The signal from PTCDA and DiMe-PTCDI internal modes remains visible even for a metal coverage of 43 nm, with higher intensity compared to the pure organic film. For Ag deposition onto DiMe-PTCDI no saturation of the signal intensity was observed up to a coverage of 263 nm.

Considering that I_0 is the intensity of the light incident on the sample, d is the nominal thickness of the metal coverage and δ is the light penetration depth in the metal, the light intensity I scattered by the sample can be described by:

$$I \propto I_0 \cdot e^{-2\frac{d}{\delta}} \qquad (1)$$

A summary of the values obtained from the fitting of the experimental decay of the enhancement factors for the totally symmetric C=C stretching mode in all investigated heterostructures is given in table 1. The obtained values are much larger compared to the penetration depth of 488 nm light into smooth closed metal films. This is a clear indication that In and Ag films grown on PTCDA and DiMe-PTCDI are not closed and have a high degree of roughness. The apparent light penetration depth in Mg films grown on PTCDA and DiMe-PTCDI estimated from the decrease in intensity of the C=C stretching mode has values comparable with the penetration depth in a closed smooth Mg film. This indicates that the Mg film is smoother and that the efficiency of the 488 nm radiation in exciting dipolar resonances is lower for Mg. The AFM topographic images in Fig. 9 confirm the higher roughness of In compared to that of Mg films.

Table 1 Skin depth of smooth metallic films, apparent penetration depth of 488 nm light in In, Ag and Mg films grown on DiMe-PTCDI and PTCDA.

	In	Ag	Mg
$\delta_{\lambda = 488\ nm}$ smooth metal film	8 nm	2.5 nm	14 nm
$\delta_{\lambda = 488\ nm}$ (DiMe-PTCDI)	49 nm	50 nm	15 nm
$\delta_{\lambda = 488\ nm}$ (PTCDA)	98 nm	-	24 nm

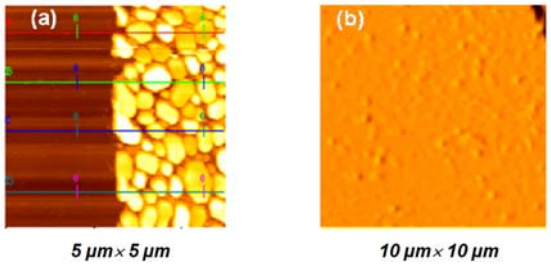

Fig. 9 AFM topographic images of a 30 nm thick In film on PTCDA (a) (the left part of the image corresponds to the substrate and the right part of the image corresponds to the In film grown on PTCDA) and of a 113 nm thick Mg film on PTCDA (b).

To recall, the A_g modes are enhanced via the long range electromagnetic effect, while the activation of B_u

modes is characteristic for the molecules in intimate contact with the metal. Therefore the intensity of B_u modes relative to that of A_g modes will be considered in the following to extract the metal diffusion depth into the organic films.

In the case of Ag/PTCDA and Ag/DiMe-PTCDI the intensity of B_u modes is relatively low, indicating that only few molecules have intimate contact with Ag. This leads to the conclusion that Ag atoms diffuse very little into PTCDA layers. On the other hand, the B_u bands are stronger compared to the A_g modes in the spectra of In/PTCDA. This suggests that a large number of PTCDA molecules have intimate contact with the metal indicating a strong diffusion of In into PTCDA layers. In/DiMe-PTCDI represent an intermediate case between Ag/PTCDA and In/PTCDA.

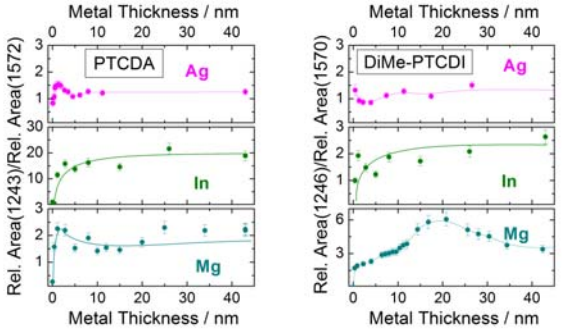

Fig. 10 Ratio between enhancement factor of the B_u mode (1243 cm^{-1} in PTCDA and 1246 cm^{-1} in DiMe-PTCDI) and of the C-C stretching A_g mode (1572 cm^{-1} in PTCDA and 1570 cm^{-1} in DiMe-PTCDI) as a function of the metal coverage.

The ratio between the area of the B_u mode at 1243 cm^{-1}(1246 cm^{-1}) and that of the A_g mode at 1572 cm^{-1}(1570 cm^{-1}) in PTCDA (DiMe-PTCDI) is shown as a function of metal thickness in Fig. 10. In the case of Ag/DiMe-PTCDI the maximum value is observed for the first Ag deposition, *i.e.* 0.4 nm Ag, whereas for PTCDA it increases up to a 1.3 nm nominal coverage of Ag. For In deposition onto both organics this ratio shows a saturation tendency only above 15 nm nominal In coverage, but its value is lower for In/DiMe-PTCDI. It is proposed that a maximum in the above defined ratio can be directly related to the metal diffusion length in the organic film. Thus the Ag atoms arriving at the organic film surface diffuse into the PTCDA islands up to a nominal Ag coverage of 1.3 nm.

For metal coverages at which the enhancement of the Raman signal due to dipolar plasmon resonances is observed, the B_u bands at around 1606 cm^{-1} (in both PTCDA and DiMe-PTCDI) become asymmetric towards the low frequency side in all the investigated systems except for Mg/PTCDA. This line-shape asymmetry is likely to be related to a Fano resonant coupling between the molecular electronic levels and the plasmons in the metallic clusters modulated by the molecular vibrations [21]. Interestingly, the mode at 1606 cm^{-1} stems from a breathing mode of the carbon rings.

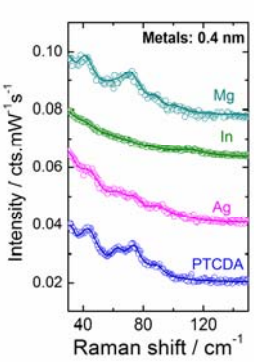

Fig. 11 Raman spectra of 15 nm thick PTCDA films covered with Ag, In and Mg in the region of the external modes.

This observation reinforces the conclusion that the interaction between the considered metals and PTCDA (DiMe-PTCDI) takes place via the perylene core.

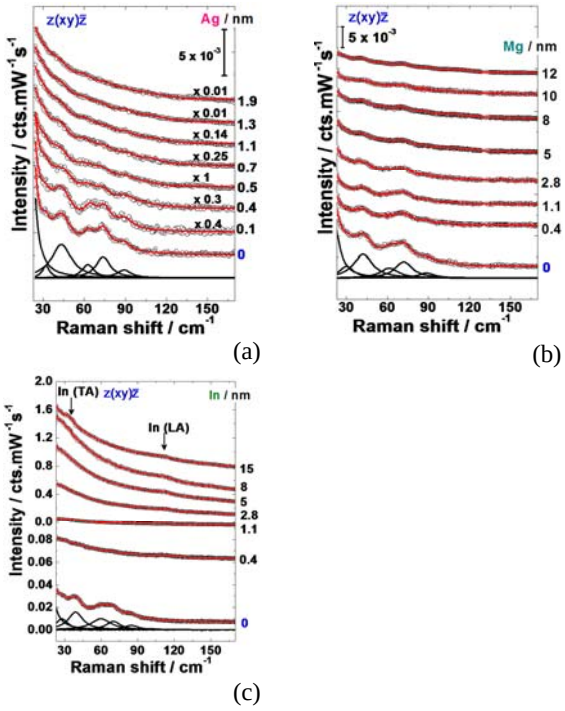

Fig. 12 Raman monitoring in the external mode region upon metal deposition: Ag (a), Mg (b), and In (c). The experimental spectra are shown by open symbols and the fitted spectra by red lines. The Lorentzian functions used for curve fitting of the Raman spectrum of the pure PTCDA film are shown by lines in the lower part of the Fig.s. The spectra are normalized for Ag/PTCDA for a better observation of the phonons.

The conclusions regarding diffusion of the metal atoms into the organic polycrystalline layers drawn from the enhancement factors of the internal modes are further confirmed by the spectral changes in the region of external modes of the organic layers. The external modes of PTCDA disappear almost completely already after depositing 0.4 nm In, while they only get broader and decrease in intensity after Ag and Mg deposition (Fig. 11).

In Fig. 12 the spectra of the external modes are shown upon step-wise metal deposition onto 15 nm of PTCDA. For a quantitative evaluation the spectra of Ag/PTCDA and Mg/PTCDA were fitted using Lorentzian functions.

The evolution of the FWHM as a function of Ag and Mg thickness is plotted in Fig. 13 for the external mode at 41 cm^{-1}. This mode is fairly well separated from its neighbours and hence the fitting parameters of the corresponding Lorentzian function are less correlated. As the metal thickness increases, the FWHM of the external modes increases faster in Ag/PTCDA compared to Mg/PTCDA.

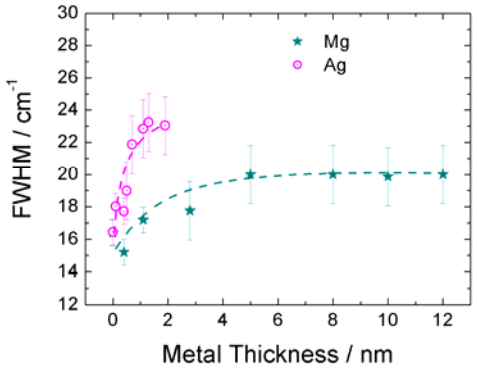

Fig. 13 Evolution of the FWHM of the external mode at 41 cm^{-1} as a function of the metal coverage relative to the initial values before the metal deposition: for Ag (a) and Mg (b). The dashed lines are guide for the eyes.

For Mg the external modes are still visible at 12 nm coverage, whereas they are almost completely smeared out at 1.3 nm of Ag. This is a clear indication that the crystalline structure of the organic layers is less affected by the Mg deposition compared to Ag. However, it should be noted that curve fitting of the spectra in the case of Ag/PTCDA is complicated by the significant increase in the low frequency background (which was already subtracted in Fig. 11). The background evolution reflects an increasing degree of roughness, which is consistent with an increasing number of metallic clusters that diffusely scatter the light. A strong increase in the low frequency background is also observed for the case of In deposition onto PTCDA, while it hardly affects the spectra of Mg/PTCDA, supporting the conclusion that the roughening due to Mg is lower compared to that of the Ag and In.

While the external molecular modes disappear already in the first deposition stages for In/PTCDA, two new modes develop at 33 cm^{-1} and 112 cm^{-1} above In coverage of 2.8 nm. They may correspond to the transverse acoustic and longitudinal acoustic phonons located at 34 cm^{-1} and 114 cm^{-1}, respectively, in bulk indium [22,23] activated due to the low dimension of the In clusters. This observation corroborated by the concomitant increase in the low frequency background indicates the formation of metallic In clusters. Moreover, the enhancement of the internal modes also increases dramatically above 2.8 nm In, supporting the conclusion of metallic cluster formation.

In the case of Mg deposition onto DiMe-PTCDI the external modes are attenuated only for a Mg nominal coverage above 21 nm (Fig. 14), *i.e.* similar to the case of Mg/PTCDA, indicating that the Mg atoms do not protrude into the crystalline molecular islands. However, the ratio between the area of the B_u mode at 1246 cm^{-1} and that of the A_g mode at 1570 cm^{-1} (Fig. 10) continuously increases up to about the same coverage. These two observations might seem contradictory when recalling the previous discussion on the correlation between the evolution of this ratio and the diffusion of the metal atoms. On the other hand, the relative intensities of the GaAs related features change already for low Mg coverages (Fig. 14) reflecting a change in the GaAs band bending. This can only occur if the Mg atoms reach the GaAs surface in the large voids between the DiMe-PTCDI islands and react with it as also learned from the PES results [2].

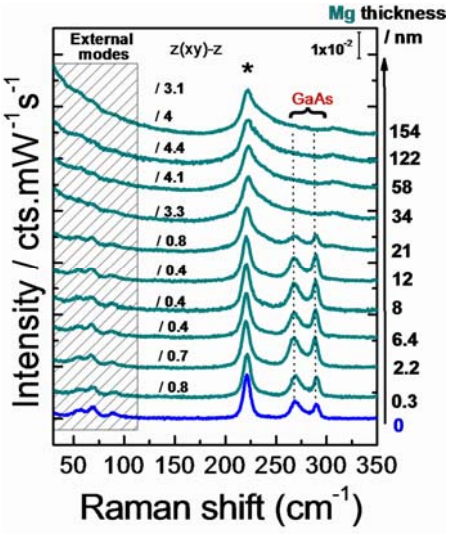

Fig. 14 Raman spectra of DiMe-PTCDI upon Mg deposition in the region of external modes and GaAs phonons. The spectra are normalized with respect to the intensity of the breathing mode at 221 cm^{-1}.

3.3 Assignment of Raman intensities with DFT calculations

As discussed in Sec. 2.2, the deformation between the geometries in the relaxed excited state of the molecule and the ground state is the key to an understanding of the elongations of different internal vibrations. The projection of this deformation pattern onto the vibrational eigenvectors yields the respective Huang-Rhys factors S_j of the mode at the frequency ω_j. Concerning linear absorption, the intensities of the vibronic subbands are governed by a Poisson progression, $P_n=e^{-Sj}/S_j^n/n!$, as observed *e.g.* for monomers in the gas phase or in weakly interacting surroundings like superfluid He [24,25]. The intensities of vibronic bands involving several internal vibrations can be calculated from the product of their respective Poisson progressions.

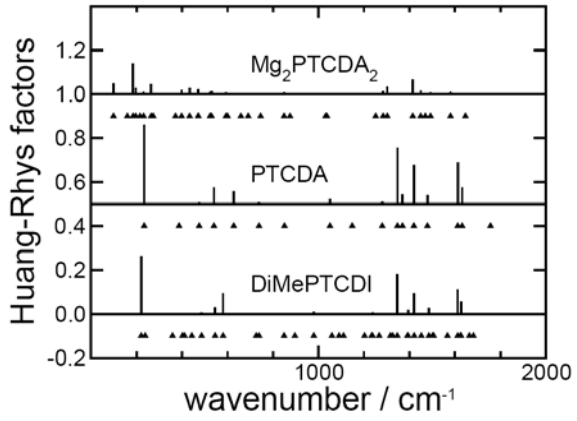

Fig. 15 Calculated Huang-Rhys factors for DiMePTCDI, PTCDA, and a nonplanar Mg_2PTCDA_2 compound visualized in Fig. 16. In all cases, the geometries have been optimized with B3LYP/DZ, and the Huang-Rhys factors are based on excited state geometries obtained with time-dependent DFT at the same level. For each compound, the positions of all breathing modes are indicated by triangles. The reference lines for the Huang-Rhys factors are shifted for clarity.

The resonant Raman intensities are determined by the same Huang-Rhys factors as $I_j \propto S_j\omega_j^2$ to leading order. Therefore, when comparing two internal modes with similar Huang-Rhys factors, the mode at the higher frequency looks more prominent in the resonant Raman spectra, compare e.g. the PTCDA breathing modes at 233 and 1303 cm^{-1}. The Huang-Rhys factors calculated with turbomole5.7 using the B3LYP functional and a double-ζ (DZ) basis are shown in Fig. 15 for PTCDA, DiMePTCDI, and Mg_2PTCDA_2 in the geometry visualized in Fig. 16.

For PTCDA, the modes with the largest calculated Huang-Rhys factors compare favourably with the observed resonant Raman spectra. More specifically, we found the following correspondence between the most prominent calculated (observed) breathing modes: 233 (233) cm^{-1}, 540 (537) cm^{-1}, 627 (624) cm^{-1}, 1347 (1303) cm^{-1}, 1369 (1347) cm^{-1}, 1412 (1379) cm^{-1}, 1612 (1572) cm^{-1}, and 1632 (1492) cm^{-1}. As expected, the B3LYP functional gives very precise values for the low frequency modes because the harmonic approximation used for the diagonalization of the dynamical matrix has only a minor influence. For high frequency modes, on the other hand, the harmonic approximation leads to an overestimate by about 3 percent with respect to the observed frequencies, a deficiency which is usually eliminated by scaling the calculated mode frequencies by a factor of about 0.97.

For DiMePTCDI, formally the smaller point group C_{2h} allows 46 breathing modes. However, when comparing PTCDA and DiMePTCDI, the most strongly elongated modes have a clear correspondence, *e.g.* for the lowest breathing mode at 220 (221) cm^{-1} in DiMePTCDI with respect to 233 (233) cm^{-1} in PTCDA. In general, for DiMePTCDI, the correspondence between calculated and observed intensities is again quite remarkable, with few exceptions, *e.g.* for pairs of vibrations very close in frequency, like the two observed modes at 1290 and 1301 cm^{-1} where the calculated Huang-Rhys factor for the lower of the two modes is much too small. However, such a borrowing of intensities between modes close in frequency could also be the consequence of inter-molecular interactions in the crystalline phase, so that the wrong relative intensity of the two modes does not necessarily indicate a principal failure of the TD-DFT approach.

In the search for useful compounds based on PTCDA and Mg, we have investigated a planar object with 4 Mg atoms surrounding the molecule in a fashion resembling Fig. 5 for In_4PTCDA, and a molecule with one Mg atom attached to each end. However, none of these candidates showed a substantial binding energy, so that we presume that they do not play any role. Moreover, due to steric hindrance between neighbouring coplanar molecules and additional Mg atoms, such candidates are highly improbable.

Instead, we have realized that pairs of intercalated Mg atoms produce a substantial binding energy of -3.9 eV in the geometry visualized in Fig. 16, and from the Mulliken charges we conclude that the net charge on the Mg sites is close to Mg^{+1}, compensated by oppositely charged $PTCDA^{-1}$. As the B3LYP functional does not account for dispersion interactions, the Pauli repulsion and the electrostatic repulsion between negatively charged PTCDA sheets are not counterbalanced by the van der Waals attraction, so that they repel each other substantially. However, in an extended model of this kind, the Ewald sums over the electrostatic interactions would still be favourable, and the Mg ions could then also connect adjacent PTCDA stacks, as proposed recently for potassium [26]. Due to the deficiencies of the B3LYP functional, we do not consider our model geometry to be realistic, but it merely represents the smallest finite size object reproducing the main features of the chemical binding of intercalated metal ions to pairs of stacked molecules.

From the Huang-Rhys factors of this Mg_2PTCDA_2 compound shown in Fig. 15, we expect substantial resonant Raman intensities in regions where the PTCDA molecules do not show any breathing modes. This reproduces the observed trends, so that despite the limitations of the DFT geometry, our finite size approximant to Mg intercalation demonstrates that chemical interaction is necessary to produce substantial changes in the vibrational signature observed in resonant Raman.

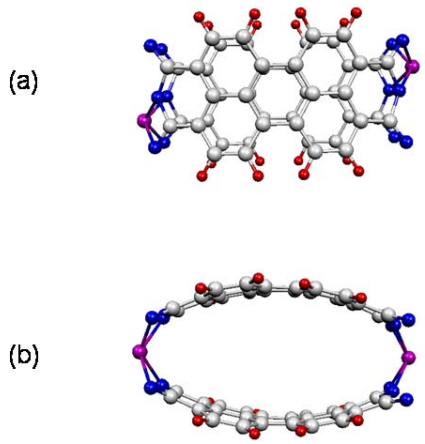

Fig. 16 Model geometry of intercalated Mg ions, optimized at the B3LYP/DZ level, a) perspective view along the molecular normal, b) view along a crystal plane. This geometry was used for the calculation of the Huang-Rhys factors visualized in Fig. 15.

4 Conclusion

The deposition of several metals with different reactivity onto thin films of perylene-derivatives was monitored *in situ* by means of resonant Raman spectroscopy. Theoretical calculations of the resonant Raman spectra describe well the observed experimentally observed frequencies of the perylene-derivatives and enable thus a reliable assignment of the Raman modes, which is essential for the understanding of the chemical aspects of the interface formation. Raman spectroscopy has shown that Ag and In behave similarly in terms of chemical reactivity when deposited onto PTCDA and DiMe-PTCDI. Both metals induce a break-down of selection rules which was interpreted as a result of a dynamical charge transfer process. The vibrational signature of Mg deposited onto PTCDA is very different compared with the other metals, indicating that a strong chemical interaction between the two partners takes place. From investigations involving one or two PTCDA molecules and two to four Mg atoms, we found that intercalated Mg ions have a favourable binding energy. In such a model for intercalation, relatively large Huang-Rhys factors in regions where PTCDA does not have any breathing modes indicate that chemical interactions are a necessary condition for the dramatic changes of the resonant Raman intensities observed after evaporation of Mg onto PTCDA films.

Upon the Ag and In deposition the totally symmetric modes are initially strongly enhanced. Subsequently the signal is attenuated exponentially with an exponent that is much smaller than the penetration depth of the incident radiation in a smooth closed metal film, reflecting a high level of roughness of the metal overlayer. On the other hand, the intensity of the normally infrared active modes relative to the Raman modes provides information on the metal diffusion depth in the organic films.

Acknowledgements This work was financially supported by the Deutsche Forschungsgemeinschaft within the OFET-SPP (Project No. SPP1121/Za146/14-2).

References

[1] G. Salvan, D. A. Tenne, T. U. Kampen, R. Scholz, G. Jungnickel, T. Frauenheim, and D. R. T. Zahn, Appl. Surf. Sci. **179,** 113 (2001).
[2] D. R. T. Zahn, G. N. Gavrila, and G. Salvan, Chem. Rev. **107,** 1161 (2007).
[3] R. Scholz, A.Yu. Kobitski, T.U. Kampen, M. Schreiber, D.R.T. Zahn, G. Jungnickel, M. Elstner, M. Sternberg, and T. Frauenheim, Phys. Rev. B **61**, 13659 (2000).
[4] R. Scholz, *Organic Semiconductors*, in: *Encyclopedia of Condensed Matter Physics*, ed. by G. Bassani, G. Liedl, and P. Wyder, Elsevier (Oxford 2005).
[5] Gaussian'98 (Revision A.1), M. J. Frisch, G. W. Trucks, H. B. Schlegel et al., Gaussian, Inc., Pittsburgh PA, **1998**.
[6] R. Ahlrichs, M. Bär, M. Häser, H. Horn and C. Kölmel, Chem. Phys. Lett. **162**, 165 (1989).
[7] A. Yu. Kobitski, R. Scholz, and D. R. T. Zahn, J. Molec. Struct. (Theochem). **625,** 39 (2003).
[8] G. Salvan, D. A. Tenne, T.U. Kampen, R. Scholz, G. Jungnickel, Th. Frauenheim, and D. R. T. Zahn, Appl. Surf. Sci. **179**, 113 (2001).
[9] D. R. T. Zahn, G. Salvan, B. A. Paez, and R. Scholz, J. Vac. Sci. Tech. A **22,** 1482 (2004).
[10] F. Brouers, S. Blacher, A. N. Lagarkov, A. K. Sarychev, P. Gadenne and V. M. Shalaev, Phys. Rev. B **55**, 13234, (1997).
[11] J. A. Creighton, Spectroscopy of Surfaces, edited by R. J. Clark and R. E. Hester, John Wiley and Sons Ltd. (1988).
[12] A. Otto, I. Mrozek, H. Graborn, W. Akemann, J. Phys.: Condens. Matter. **4**, 1134 (1992).
[13] K. Kneipp, H. Kneipp, I. Itzkan, R. R. Dasari, M. S. Feld, Chem. Rev. **99**, 2957 (1999).
[14] A. Otto, phys. stat. sol. (a), **188-189**, 1455 (2001).
[15] A. Otto, I. Mrozek, H. Graborn, W. Akemann, J. Phys.: Condens. Matter. **4**, 1134 (1992).
[16] A. Yu. Kobitski, G. Salvan, R. Scholz, D. Tenne, T. U. Kampen, H. P. Wagner, D. R. T. Zahn, Appl. Surf. Sci. **190**, 386 (2002).

[17] G. Salvan and D. R. T. Zahn, Europhys. Lett. **67**, 827 (2004).
[18] Y. Hirose, A. Kahn, V. Aristov, P. Soukiassian, V. Bulovic, S.R. Forrest, Phys. Rev. B **54**, 13748 (1996).
[19] S. Kera, H. Setoyama, M.Onoue, K. Okudaira, Y. Harada, N. Ueno, Phys. Rev. B **63**, 115204 (2001).
[20] H. K. Böckelmann and R. G. Schlecht, Phys. Rev. B. **10**, 5225 (1974).
[21] B.A. Paez, G. Salvan, R. Scholz, D. R. T. Zahn, phys. stat. sol. (c). **2**, 4048 (**2005)**.
[22] K. Fleischer, S. Chandola, N. Esser, W. Richter, and J. F. McGilp, Phys. Rev. B **67**, 235318 (2003).
[23] A. S. Bakulin, A. W. Overhauser, H. Kaiser, S. A. Werner, J. A. Fernandez-Baca, H. G. Smith, Phys. Rev. B **63**, 052301 (2001).
[24] M. Wewer and F. Stienkemeier, Phys. Rev. B. **67**, 125201 (2003).
[25] R. Scholz and M. Schreiber, Chem. Phys. **325**, 9 (2006).
[26] C. Zazza, S. Meloni, A. Palma, M. Knupfer, G. G. Fuentes, and R. Car , Phys. Rev. Lett. **98**, 046401 (2007).